Transformer Design Optimization and Comparison for a DC-DC Converter used in PV Micro-Inverters

Tobias Manthey, Meriem Khader, Jens Friebe
Institute for Drive Systems and Power Electronics
Leibniz University Hannover
Email: tobias.manthey@ial.uni-hannover.de; friebe@ial.uni-hannover.de

Acknowledgement

Parts of this work were funded by the German Federal Ministry for Economic Affairs and Energy under Grant No. 03EE1057A (Voyager-PV) and also by the Ministry of Science and Culture of Lower Saxony and the Volkswagen Foundation. The authors are responsible for the content of this publication.

Keywords

≪Transformer≫, ≪Passive component≫, ≪Resonant converter≫, ≪ZVS converter≫, ≪Isolated converter≫

Abstract

The use of micro-inverters can lead to higher efficiency of photovoltaik systems, since shading problems and system failures have only a small impact. The most significant component in terms of losses and moreover extensive in the design process is the transformer which is necessary for the galvanic isolation and topology-dependent voltage boost. This paper compares several optimization options, both simulatively and through measurement-based verification.

Introduction

The availability of grid-connected micro-inverters has increased greatly in recent years and with it the demand for more and more efficient systems [1]. Since the semiconductor losses have an increasingly smaller proportion of the total losses due to soft switching, the transformer losses can have the greatest influence on the efficiency [2], [3]. However, transformers are required for the galvanic isolation between photovoltaic (PV) modules and the grid as well for voltage level transformation required for grid feeding. High currents, high switching frequencies and increasing power class of photovoltaic modules are challenging for the transformer design in terms of efficiency, temperature rise, volume and costs [4]. A fundamental design approach and an overview of magnetic materials as well as windings are given in [5] and [6].

In this paper, design criteria and parameter variations are discussed and performed based on simulations and measurements of a given hardware prototype of a series resonance converter (SRC) topology used in micro-inverters with an output power of 500 W and a switching frequency of 500 kHz serves as an application example. As a result of the extensive analysis of the topology and the operating point slightly below resonant frequency, the following section examines the influence of different core shapes as well as different winding materials and arrangements while keeping the core material and turn ratio constant. A major part of the simulations is performed with the artificial intelligence based software Frenetic, supported by investigations within a 2D FEM environment. In the last section, the measurement results are compared and analysed using efficiency curves of the entire set-up with the different transformers. For additional verification of the simulated core and winding losses, thermal images are taken with an IR camera.

Topology Description and Hardware Setup

First, a brief investigation of the influence of magnetizing inductance on the switching behavior is presented and the general conditions for the hardware prototype are listed in Table I. Fig. 1 shows the circuit diagram of the series resonant converter and the analyzed voltage and current characteristics. The objective is to discharge the output capacitance C_{OSS} of each MOSFET within the dead time to achieve zero voltage switching (ZVS) using the magnetizing current. Fig. 2 shows the simplified current and voltage waveforms for the possible operating points above and below resonance. The operating point $f_{sw} = f_{res}$ is not taken into account, as the operating point can shift under temperature and other external influences, since the proposed hardware prototype is an open loop system. In order to minimise the losses in the power semiconductors, the operating point shown in Fig. 2 (a) is preferred. In addition to ZVS in the primary-side MOSFETs, zero current switching (ZCS) at turn-off transition is also achieved in the diodes as the resonance is already completed before the switching transition. The challenge here is to design the transformer with a magnetizing inductance that is small enough to achieve a sufficiently high magnetizing current to discharge the output capacitances C_{OSS} in the switches within the deadtime. Fig. 9 shows the current and voltage waveforms for $L_m = 4\,\mu H$ and $L_m = 7\,\mu H$, in which ZVS is achieved only with the smaller inductance due to the higher magnetizing current. A further reduction of the magnetizing inductance enables a shorter dead time but also would lead to a higher current stress on the MOSFETs. An analysis of the trade off of dead time and ZVS was analyzed as an example in [7].

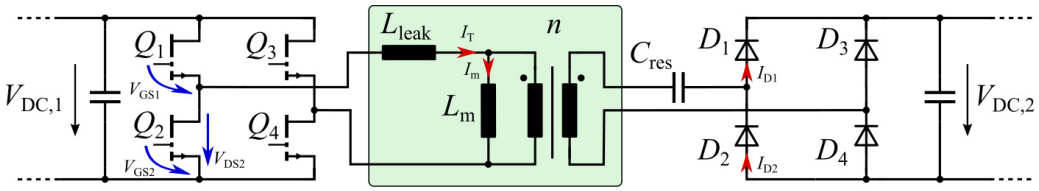

Fig. 1: Circuit description of the series resonant converter and color highlighting of the transformer.

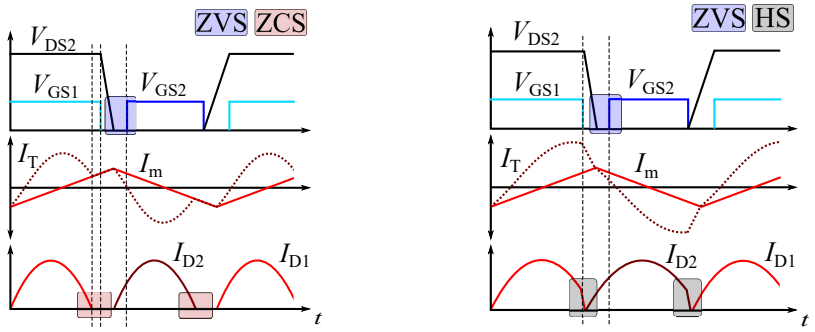

(a) Primary MOSFETs achieve ZVS at turn-on transistion and secondary rectifier diodes achieve ZCS when turning off.

(b) Only ZVS is achieved on the primary side MOSFETs. The diodes will be turned of with hard-switching (HS) due to the lagging current.

Fig. 2: Simplified waveforms of voltages and currents marked in Fig. 1. The operating point in (a) is preferred because of ZVS and ZCS.

To keep the magnetic components of the prototype as small as possible, the switching frequency is defined at 500 kHz, which has been tested to be acceptable for the switching losses of the primary and secondary side power semiconductors. In addition the leakage inductance of the transformer is used as the resonance inductance, which in combination with the resonance capacitance leads to the resonance frequency of the SRC defined in equation 1. The second resonance frequency, which results from the sum of the two inductances, is located far enough away from the operating point that it cannot be seen in

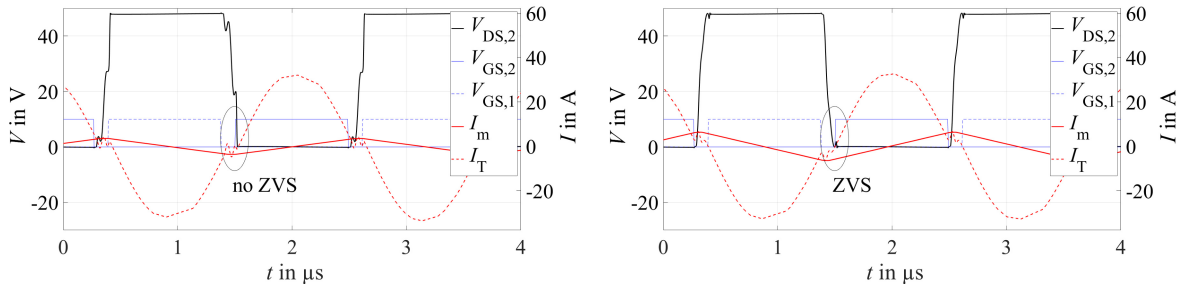

(a) L_m = 7 µH, hard-switching

(b) L_m = 4 µH, soft-switching

Fig. 3: Simulative switching behaviour of the primary MOSFETs with two different values of magnetizing inductance. The switching frequency is 500 kHz and the dead time between the gate signals is set to 130 ns.

the transfer function of the series resonance converter.

$$f_{\text{res},1} = \frac{1}{2\pi \cdot \sqrt{L_{\text{leak}} \cdot C_{\text{res}} \cdot n^2}} > f_{\text{sw}} \qquad f_{\text{res},2} = \frac{1}{2\pi \cdot \sqrt{(L_{\text{leak}} + L_{\text{m}}) \cdot C_{\text{res}} \cdot n^2}} << f_{\text{res},1} \tag{1}$$

For the measurement of the transformers, a setup consisting of two PCBs, divided into primary and secondary side of the transformer, is designed, shown in Fig. 4. Consisting of two half-bridges equipped with Si MOFETs BSC025N08LS from Infineon, which are controlled via a gate driver and an external microcontroller for setting the switching frequency. A drain-source voltage measurement is implemented in the gate driver so that the dead time for reaching ZVS is adjusted by the driver itself. Large soldering pads for contacting the transformer offer the possibility to create a solder or screw connection. On the secondary side, next to the connection points, is the resonance capacitor which is realised with C0G capacitors to avoid a shift of the operating point because of voltage or temperature changes. Furthermore the different transformer designs result in different leakage inductances, which means that the resonance capacitance must be adjusted for each transformer. For this purpose, it is possible to connect several capacitors in parallel in order to be able to measure the design with a minimum leakage inductance of 22 nH. A full bridge diode rectifier with SiC Schottky diodes and an output capacitor provide the DC voltage on the output side. With the nominal input voltage of 48 V, the switching frequency of 500 kHz and a constant duty cycle of 50 %, an initial approximation of the magnetic flux density within the core can be estimated using equation 2, considering a triangular magnetizing current. The second DC-link voltage should be high enough to provide the negative and positive half-waves of the grid voltage using an inverter. A value of 384 V is chosen which can be realised with a transformer turn ratio of n = 8.

$$\hat{B} = \frac{V_{\text{DC},1}}{4 \cdot f_{\text{sw}} \cdot n_{\text{prim}} \cdot A_{\text{e}}} \tag{2}$$

Transformer Design Process and Comparison

The idea of the design process is to change only one parameter at a time in order to identify the influence of the different degrees of freedom in the transformer design and focusing on methods to reduce losses and maximum temperatures as well as cost and volume optimization. For this approach, the core material and the secondary winding type are identical in each design and only the primary winding and its parameters as well as the core shape are varied. The N49 ferrite core material is the most suitable in the given frequency range [8] and is available for all cores considered in the simulation. With regard to the availability of core shapes on the market, the choice of cores is initially limited. Due to the high current on the primary side and the high switching frequency, the losses of the primary winding are dominant, so litz winding with a single strand diameter of 0.1 mm and 100 single wires can be selected for the secondary winding and is used in all designs for better comparability.

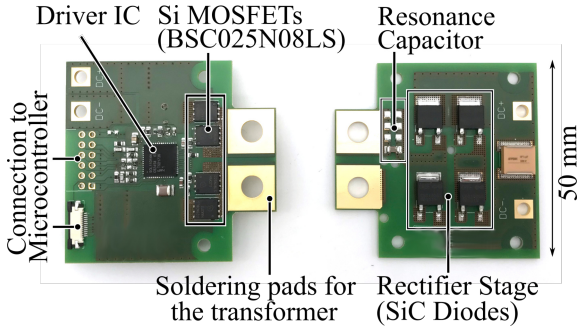

Fig. 4: Photograph of the 500 W hardware prototype without the transformer.

Table I: General conditions for the design of the transformer and fixed parameters.

Parameters	Symbol	Value
Input voltage	$V_{DC,1}$	48 V
Output voltage	$V_{DC,2}$	384 V
Rated output power	P_{out}	500 W
Switching frequency	f_{sw}	500 kHz
Resonance frequency	f_{res}	515 kHz
Turns ration	n	8
Core material		N49
Secondary winding		100 x 0.1 mm

Table II shows all the compared transformer designs as well as the design parameter changes. Overall, the influence on the core shape, primary turns, winding arrangement and winding type is investigated. A winding interleaving from PSS to SPS has only a small influence on the winding losses, but can be realised with little effort. Adding another turn on the primary side has a greater influence on the total losses. Although the winding losses increase, the core losses are reduced by a multiple. To reduce the increased winding losses, a litz wire winding with a smaller wire cross-section can be used. In this example a change from 50 µm (highlighted in green) to 30 µm (highlighted in blue) diameter leads to a reduction in winding losses of about 300 mW by keeping the total copper cross-section almost identical for both windings. The use of foil winding (highlighted in yellow) at first leads to higher losses simulatively, however, this will not show up in the measurements as it can be seen in the next section. In addition, foil winding is both less expensive and has a higher copper fill factor. Core shapes with larger core cross-sections and winding windows offer the possibility of further increasing the number of windings. However, since the winding losses increase more than the core losses decrease, this does not offer any optimization. The step towards larger cores offers no further advantages in this frequency and power range, and costs and construction volume can be saved.

Table II: Design parameters and simulation results of the individual transformers at 500 W and natural convection. Primary litz winding is marked in green and blue for 50 µm and 30 µm litz diameter as well as foil winding marked in yellow. Additional parameter changes are labeled on the side of the table.

Nr.	Core	w.a.	n_{prim}	P_c	P_w	P_{tot}	
1:	PQ 32/30	PSS	2	2.82 W	0.51 W	3.33 W	W. arrangement
2:	PQ 32/30	SPS	2	2.80 W	0.30 W	3.10 W	n_{prim}
3:	PQ 32/30	SPS	3	0.27 W	1.19 W	1.46 W	Litz parameters
4:	PQ 32/30	SPS	3	0.27 W	0.88 W	1.15 W	
5:	PQ 35/35	PSSS	2	1.79 W	1.19 W	2.98 W	W. arrangement
6:	PQ 35/35	SSPS	2	1.74 W	0.82 W	2.56 W	
7:	PQ 32/20	SPSS	2	3.02 W	0.69 W	3.71 W	Core & arragem.
8:	RM 14	SPS	2	2.50 W	0.50 W	3.00 W	Winding type and n_{prim}
9:	RM 14	SPS	3	0.68 W	3.24 W	3.92 W	
10:	PQ 40/40	SPSP	4	0.41 W	2.12 W	2.53 W	W. arrangement
11:	PQ 40/40	PSPS	4	0.38 W	2.24 W	2.62 W	

Core & winding type: Core (1–4), Core (7–9)

Transformer Prototypes and Measurement Verification

A part of the transformer prototypes are shown in Fig. 6. To achieve comparability of the overall system and to identify the transformer losses, the magnetizing inductance of each design is adjusted to about 4 µH by changing the air gap to ensure ZVS. The resonance frequency is set via the resonance capacitance, as each design has a different value of leakage inductance. Since only the overall system can be measured for the efficiency measurement, but the influence of the power semiconductors is not of interest, the difference in total power dissipation between the various designs is compared with the difference of transformer losses from the simulation results. The efficiency measurement of the four transformer prototypes is shown in Fig. 7 as well as voltage and current waveforms in Fig. 8 as an example resulting from the hardware setup with transformer No. 1 in which ZVS is achieved. The crosses in the efficiency measurement mark the measurement result after the steady state has been reached. Initial measurement investigations are relate to the arrangement of the foil winding, which in the PQ32/20 core has to be implemented in two layers due to its size, whereas the RM14 core offers the option of placing the windings on top of each other, as shown in Fig. 5 (b). After a 30-minute steady-state period, a maximum efficiency of 97.58 % was achieved with the PQ32/20. In order to compare only the difference in power loss, Table III include both, differences of the simulation results ΔP_{sim} as well as the differences of the measurement results ΔP_{meas}. It is observed that the transformers prototypes with the same primary winding, the simulations achieve well-matched results compared to the measurements. Since the simulation and measurement results are generally very close to each other at an output power of 500 W, Table II can be used as a good reference for the effect of changing the individual design parameters.

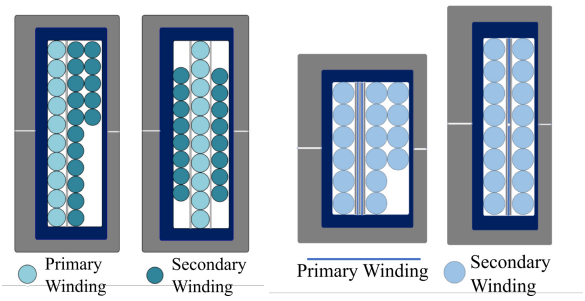

(a) PQ 32/30 (b) RM 14 (left) and PQ 32/20 (right)

Fig. 5: Schematic winding arrangement in one winding window of the core.

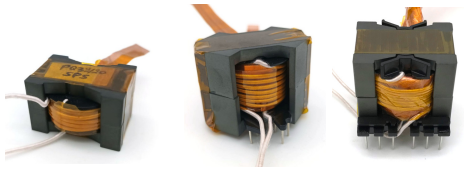

(a) PQ 32/20 (b) RM 14 (c) PQ 32/30

Fig. 6: Photographs of the first transformer prototypes.

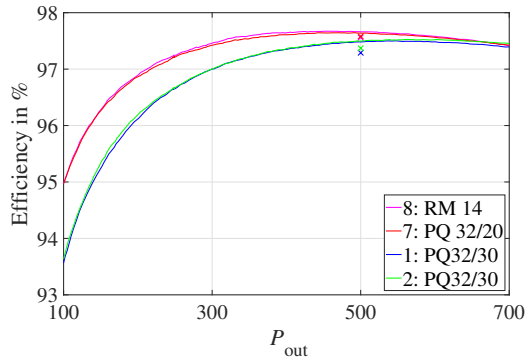

Fig. 7: Efficiency measurement of the two transformer prototypes RM 14 and PQ 32/20 with foil winding. The crosses mark the efficiency in steady state after about 30 minutes of operation.

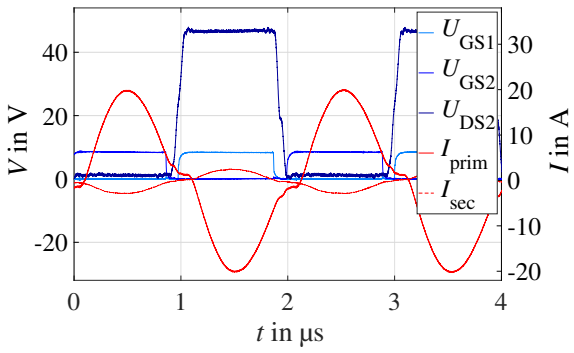

Fig. 8: Resulting waveforms of transformer No. 1 with 500 W output power. ZVS is achieved with a dead time of 128 ns as it was expected from the simulation.

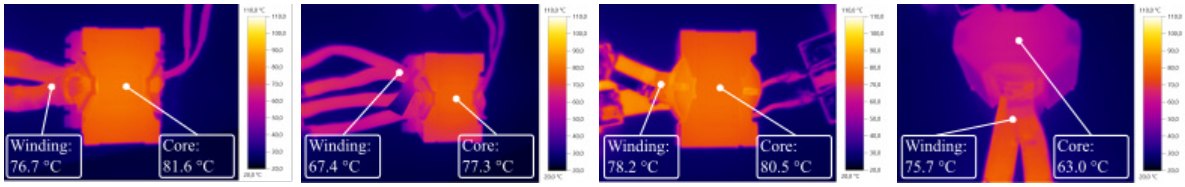

(a) Transformer 1 (b) Transformer 2 (c) Transformer 7 (d) Transformer 8

Fig. 9: Winding and core temperatures of the different transformers taken with a IR camera.

Table III: Comparison of simulation and measurement results.

Nr.	Core	w.a.	n_{prim}	P_{c}	P_{w}	P_{tot}		
1:	PQ 32/30	PSS	2	2.82 W	0.51 W	3.33 W	ΔP_{sim} = -0.23 W	$\Delta P_{\text{meas.}}$ = -0.42 W
2:	PQ 32/30	SPS	2	2.80 W	0.30 W	3.10 W	ΔP_{sim} = +0.61 W	$\Delta P_{\text{meas.}}$ = -1.11 W
7:	PQ 32/20	SPSS	2	3.02 W	0.69 W	3.71 W	ΔP_{sim} = -0.71 W	$\Delta P_{\text{meas.}}$ = -0.11 W
8:	RM 14	SPS	2	2.50 W	0.50 W	3.00 W		

Conclusion

This paper deals with the design optimization of transformers, especially for DC-DC converters for micro-inverters or other series resonant converter topologies. First, the switching behavior is simulated as a function of the magnetizing inductance. Furthermore, an analysis of operating point below and above the resonant frequency was made to show that both ZVS on the primary side and ZCS on the secondary side can be achieved. An extensive research of varying the different design parameters of the transformer to show the influence of winding and core losses was made in section . To make a comparison with the measurement results, only the difference of power loss between two transformer designs is considered in order to filter out the influence of the power semiconductors. This comparison shows that there is good correlation with the simulation results and ways of optimising the transformer design can be identified. A maximum efficiency of 97.58 % was achieved with a transformer prototype consisting out of a PQ 32/20 and two primary foil winding turns in two layers.

References

[1] J. M. A. Myrzik and M. Calais, “String and module integrated inverters for single-phase grid connected photovoltaic systems - a review,” in IEEE Bologna Power Tech Conference Proceedings, pp. 8, vol. 2, 2003
[2] T. Manthey, T. Brinker and J. Friebe, “Design of an Isolated DC-DC Converter for PV Micro-Inverters with Planar Transformer and PCB Integrated Winding,” 2021 IEEE Energy Conversion Congress and Exposition (ECCE), pp. 554-560, 2021
[3] H. Rezaei and A. Babaei, “Thermal analysis of inverters and high frequency transformers in the DC-DC converters,,” 2017 IEEE 4th International Conference on Knowledge-Based Engineering and Innovation (KBEI), pp. 0125-0130, 2017
[4] T. M. Undeland, J. Lode, R. Nilssen, W. P. Robbins and N. Mohan, “A single-pass design method for high-frequency inductors,” in IEEE Industry Applications Magazine, vol. 2, no. 5, pp. 44-51, Sept.-Oct. 1996
[5] V. C. Valchev and V. A. D. Bossche, “Inductors and Transformers for Power Electronics (1st ed.),” CRC Press, 2005
[6] P. Zacharias, “Magnetische Bauelemente: Grundlagen und Anwendungen (1st ed.),” Springer Vieweg, ISBN 978-3-658-24741-6, 2020.
[7] GaN Systems Inc., “Gate Drive Circuit Design with GaN E-HEMTs,” GN012 Application Note, 2020
[8] TDK, “Ferrites and accessories, SIFERRIT material N49,” datasheet, 2017